Simulations and Analyses of Expected Nucleon Transversity Measurements in the MINERνA Neutrino Experiment

An Honors Thesis for the Department of Physics and Astronomy

Pauli Kehayias

Tufts University, 2009

Acknowledgements

I would like to thank my committee members Bruce Boghosian, Hugh Gallagher, and Gary Goldstein – Professor Gallagher in particular for his advice and patience throughout my time at Tufts. I would also like to thank Dr. Costas Andreopoulos (Rutherford Appleton Laboratory) for help with GENIE.

Table of Contents

Abstract

Coherent charged current single pion production events were simulated and analyzed for the MINERνA neutrino experiment. The differential cross section of this reaction is transversity-dependent in the pion azimuthal angle φ according to two models: the GPD model and the Regge model. Our goal was to determine whether MINERνA will be able to differentiate between these two models. We found that the GPD model predicts an event rate largely independent of φ while the Regge model predicts a significant $\cos(2\varphi)$ contribution. MINERνA will have sufficient resolution and statistics to distinguish between the two, though a more thorough investigation is needed.

Introduction

Neutrinos are neutral elementary particles that travel at nearly the speed of light. They are much lighter than other elementary particles and interact less frequently with other matter. Neutrinos were formulated by Pauli in 1930 to resolve why beta decay reactions appeared to violate conservation of energy and were discovered in 1956 by Reines and Cowan in a nuclear reactor experiment. Neutrino experiments have studied neutrinos from natural sources (the Sun, supernovae, radioactive decay, and atmospheric cosmic ray interactions) and artificial sources (nuclear reactors and proton accelerators). Neutrinos interact rarely with other matter, making neutrino experiments difficult because of the low event rate. However, since neutrinos are a unique probe in particle physics, neutrino experiments are worth the difficulty.

MINERνA (Main Injector Experiments for ν-A) is a neutrino experiment at the Fermi National Accelerator Laboratory (Fermilab). It is still under construction but recently started taking data, and the detector and targets have a range of nuclear targets. MINERνA data will be

used to assess neutrino-nucleon cross-sections, nucleon substructure, and nuclear effects on neutrino interactions. The cross section measurements will reduce the uncertainties in neutrino experiments searching for other neutrino physics, such as flavor oscillation [1].

MINERνA data can be used for a novel nucleon substructure analysis. Nucleons consist of pointlike particles called partons, which are quarks and gluons. Their behavior is described by the quark parton model, a theory that makes predictions about the spatial and longitudinal momentum probability distributions of the quarks within the nucleon. An extension to the quark parton model that describes the transverse nucleon structure can be derived from more general mathematical objects called generalized parton distributions (GPDs). Four of the eight quark GPDs are called the transversity GPDs [2]. The term "transversity" applies to these GPDs and the effects they produce in certain reactions.

Transversity has been studied experimentally with electron and proton probes, but never with neutrino probes. MINERνA will detect coherent charged current single pion production events (such as $\nu_\mu + {}^{12}C \rightarrow \mu^- + \pi^+ + {}^{12}C$), and this reaction has transversity-dependent kinematics. The probability (differential cross section) of this reaction has trigonometric dependence on the angle φ of the final state pion momentum with respect to neutrino and muon momenta [3]. Transversity gives rise to this φ dependence, hence MINERνA will be able to attempt transversity measurements with neutrinos.

Cross sections calculated from two models (the GPD model and the Regge model) determine the relative weights of the sinusoidal φ terms [3]. Our goal is to predict whether MINERνA will be sensitive enough to the event rate variations in φ to distinguish a difference between these two models. We simulated events with and without the model φ dependence, introduced detector resolution and reconstruction effects, and examined the φ-dependent event rates and φ resolution.

We found that the Regge model predicts an event rate with a strong $\cos(2\varphi)$ component while the GPD model predicts an event rate largely flat in φ. MINERνA will be sensitive enough to this difference, though more elaborate simulations are necessary.

Theory

1. Elementary Particles and the Standard Model

The idea that matter is built from unbreakable constituents originates from ancient Greek philosophers. Finding and describing the smallest such particles continues to be a goal of modern physics. The smallest (pointlike) particles are called elementary particles, and all matter is composed of elementary particles. Similarly, all forces in nature are manifestations of the fundamental forces: the strong force, the electromagnetic force, the weak force, and gravity. Elementary particles and their interactions through the fundamental forces (except for gravity) are described by a set of theories called the Standard Model, which has been exceptionally successful at predicting experimental results. However, since it does not account for gravity, the Standard Model is an incomplete description of elementary particle interactions.

Standard Model elementary particles include six quarks, six leptons, five force carriers, and their antiparticles (Figure 1). The fundamental forces and their relative strengths are carried by the particles indicated in Table 1. Gravity and electromagnetism have infinite range and decrease as $1/r^2$, where r is the separation distance between point masses or charges. The strong and weak force ranges are on the scale of atomic nuclei.

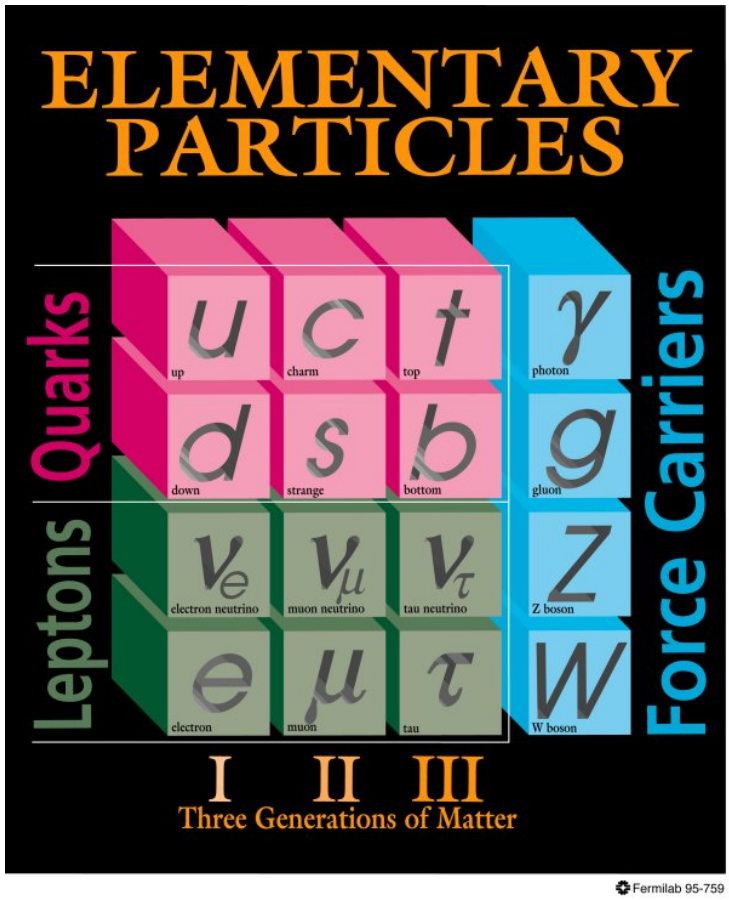

Figure 1: Elementary particles in the Standard Model. The *W* boson is in fact two particles, and the graviton is not shown [4].

Force	Relative Strength	Carrier	Carrier Symbol	Spin
Strong	1	Gluon	g	1
Electromagnetic	10^{-2}	Photon	γ	1
Weak	10^{-13}	W and Z bosons	$W^{\pm}$, Z^0	1
Gravity	10^{-42}	Graviton	G	2

Table 1: The fundamental force carriers [5].

Leptons and quarks are spin 1/2 fermions. There are three lepton types ("flavors"): electron, muon, and tau. For each lepton flavor there is a charged lepton: the electron, the muon, and the tau, and their corresponding antiparticles (Table 2). Each has a charge of $\pm e$, where $e = 1.602 \times 10^{-19}$ C. Charged leptons interact through electromagnetism, the weak force, and

gravity. Each lepton flavor has a neutral neutrino and antineutrino as well, which interact through the weak force and gravity. In weak interactions, a lepton can only transform into a lepton of the same flavor.

A particle with spin can have its spin aligned parallel or antiparallel to its direction of motion, with the former being a right-handed particle and the latter being left-handed. Almost all particles have both left and right-handed states, but (massless) neutrinos are always left-handed and antineutrinos are always right-handed. This indicates that the weak force is not parity-invariant (not identical under coordinate inversions).

Symbol	Name	Charge (e)	Mass (MeV/c^2)
e^- (e^+)	Electron (positron)	-1 (+1)	0.5110
μ^- (μ^+)	Muon	-1 (+1)	105.7
τ^- (τ^+)	Tau	-1 (+1)	1776
ν_e ($\overline{\nu}_e$)	Electron (anti)neutrino	0 (0)	
ν_μ ($\overline{\nu}_\mu$)	Muon (anti)neutrino	0 (0)	
ν_τ ($\overline{\nu}_\tau$)	Tau (anti)neutrino	0 (0)	

Table 2: Standard model leptons, with antiparticles in parentheses. Neutrino mass states are different from flavor states [6].

Subatomic particles composed of quarks are called hadrons. Nucleons and other hadrons are made of partons (quarks and gluons). There are six quark types: up, down, charm, strange, top, and bottom (Table 3). Up and down quarks are the lightest and make up protons (*uud*) and neutrons (*udd*). These are the most common quarks and compose most baryonic matter. Heavier quarks are produced in relativistic particle collisions and decay to lighter quarks by the weak force. Quarks interact through the strong force, which holds quarks together in hadrons and is carried by gluons. Quarks and antiquarks have charge $\pm 1/3e$ or $\pm 2/3e$, but are only found in

mesons (bosons with one quark and antiquark) and baryons (fermions with three quarks or antiquarks), all of which have integer charge. Isolated (free) quarks are not detectable experimentally – an empirical fact explained in the Standard Model by quark confinement. If two bound quarks are pulled apart, the binding energy between them increases to the point where a quark-antiquark pair spawns. One of the new quarks joins the separated quark to produce a new meson [5, 7]. In addition to the quarks that make up the hadron (valence quarks), extra quark/antiquark pairs (sea quarks) continuously spontaneously appear by gluon decay and annihilate [5].

Symbol	Name	Charge (e)
u ($\bar{u}$)	Up	+2/3 (-2/3)
d ($\bar{d}$)	Down	-1/3 (+1/3)
c ($\bar{c}$)	Charm	+2/3 (-2/3)
s ($\bar{s}$)	Strange	-1/3 (+1/3)
t ($\bar{t}$)	Top	+2/3 (-2/3)
b ($\bar{b}$)	Bottom	-1/3 (+1/3)

Table 3: Quarks and their charges, with antiquarks in parentheses.

The strong force interactions between quarks and gluons are described by quantum chromodynamics (QCD), which states that quarks and gluons carry "color charge" that dictates their interactions. Color takes six values: (anti)red, (anti)blue, and (anti)green. Observable hadrons are colorless, meaning that the quarks in mesons must have opposite color (for example, red and antired) and that baryons contain one quark of each color or anticolor. QCD also predicts that quarks experience asymptotic freedom, where the strong force becomes weaker at short

distances, at high energy. Asymptotic freedom allows the quarks be approximated as free particles when considering relativistic particle scattering [5].

2. Elastic Scattering and Deep Inelastic Scattering

In the Rutherford gold foil experiment, alpha particles were scattered off of gold atoms to study atomic substructure. Nucleon substructure is studied by scattering higher energy probes. With sufficiently high energy, probe particles have a short enough de Broglie wavelength to scatter off of the pointlike partons instead of the nucleus or nucleons as a whole. Elastic scattering leaves the incident particles intact while inelastic scattering does not conserve kinetic energy and produces new particles from the incident particle energies. Elastic scattering is calculable using functions called form factors. Form factors depend on the probe-target three-momentum transfer $\boldsymbol{q}$ and are the inverse Fourier transform of nucleon spatial charge distribution. Inelastic scattering off of partons is called deep inelastic scattering (DIS). The final state kinematics are described by two-parameter structure functions. Structure functions are measured in DIS experiments and provide information on how momentum along the incident probe trajectory is distributed among the partons in a nucleon [8, 9].

Neutrino-quark DIS reactions are classified into two reaction types. In charged current (CC) reactions, a $W^{\pm}$ is exchanged between the neutrino and the quark, and both acquire a new charge (the neutrino becomes a charged lepton and the quark changes type). Neutral current (NC) reactions involve a Z^0 exchange, and the incident neutrino remains a neutrino. The parameters used to describe scattering reactions are [8]:

$\boldsymbol{p}$, the incident nucleon four-momentum.
$\boldsymbol{k}$ and $\boldsymbol{k'}$, the initial and final lepton four-momenta.

$\nu = E - E'$, where E is the incident neutrino energy and E' is the resultant lepton energy (both in the lab frame).

$Q^2 = -|\boldsymbol{q}|^2 = 4EE' \sin^2(\theta / 2)$, where $\boldsymbol{q} = \boldsymbol{k} - \boldsymbol{k'}$ and θ is the scattering angle in the lab frame. $\boldsymbol{q}$ is the momentum transfer from the incident lepton to the target.

$\boldsymbol{t} = \boldsymbol{q} - \boldsymbol{p}_{had}$, where $\boldsymbol{p}_{had}$ is the hadron shower four-momentum, and $t = |\boldsymbol{t}|$. $\boldsymbol{t}$ is the momentum transfer to the target.

$x = Q^2 / (2\,\boldsymbol{p} \cdot \boldsymbol{q}) = Q^2 / (2M_n\nu)$, where M_n is the target nucleon mass. This is called the Bjorken x. x is the fraction of the incident nucleon momentum carried by the interacting quark.

$y = \boldsymbol{p} \cdot \boldsymbol{q} \,/\, \boldsymbol{p} \cdot \boldsymbol{k} = \nu / E$, which is a measure of the energy transferred from the incident lepton to the resulting hadron shower. y is related to the center of mass frame lepton scattering angle θ' by $y = (1 - \cos\theta') / 2$.

$s = |\boldsymbol{p} + \boldsymbol{k}|^2$, which is the magnitude of the center of mass four-momentum.

Of these parameters, Q^2, t, x, y, and s are Lorentz-invariant.

Scattering experiments count event frequencies to measure differential cross section, which is the probability that a reaction will occur with certain kinematic parameters. The neutrino-nucleon and antineutrino-nucleon CC differential cross sections depend on the structure functions F_1, F_2, and F_3 as follows (h represents either a proton or a neutron):

$$\frac{d^2\sigma(\nu h)}{dx\,dy} = \frac{G_F^2 s}{2\pi}\left[xy^2F_1^{\nu h}(x,y) + (1-y)F_2^{\nu h}(x,y) + y\left(1-\frac{y}{2}\right)xF_3^{\nu h}(x,y)\right]$$

$$\frac{d^2\sigma(\bar{\nu} h)}{dx\,dy} = \frac{G_F^2 s}{2\pi}\left[xy^2F_1^{\bar{\nu} h}(x,y) + (1-y)F_2^{\bar{\nu} h}(x,y) - y\left(1-\frac{y}{2}\right)xF_3^{\bar{\nu} h}(x,y)\right]$$

Neutrino and antineutrino differential cross sections are almost identical except for a difference in F_3 sign. We can exploit this fact to measure structure functions from experimental differential cross sections by taking linear combinations of differential cross sections at given y to cancel either F_2 or F_3 and solve for the other [8].

The quark parton model states that structure functions depend on the longitudinal momentum fraction probability distributions of the nucleon's quarks (including sea quarks) [8]:

$$F_1(x) = F_2(x)/2x$$

$$F_2^{\nu p}(x) = 2x\left(d(x) + s(x) + \bar{u}(x) + \bar{c}(x)\right)$$

$$F_2^{\bar{\nu}p}(x) = 2x\left(u(x) + c(x) + \bar{d}(x) + \bar{s}(x)\right)$$

$$xF_3^{\nu p}(x) = 2x\left(d(x) + s(x) - \bar{u}(x) - \bar{c}(x)\right)$$

$$xF_3^{\bar{\nu}p}(x) = 2x\left(u(x) + c(x) - \bar{d}(x) - \bar{s}(x)\right)$$

The parton distribution function (PDF) $q(x)$ is the probability distribution for finding a quark of type q with longitudinal momentum fraction x. Sea quarks are responsible for the charm, strange, and antiquark terms. We assume that the incident neutrinos considered have sufficient energy to scatter off of c quarks, but not t or b quarks. Structure functions have no q^2 dependence because of Bjorken scaling, which shows that structure functions depend on x only as $Q^2 \rightarrow \infty$. QCD introduces a ln Q^2 dependent correction to Bjorken scaling [8].

The ν and $\bar{\nu}$ structure functions have opposite quark types for each generation because a νp (or $\bar{\nu}p$) reaction requires that the quark absorb a W^+ (W^-), which can only occur for quarks of negative (positive) charge. Structure functions and quark PDFs are conventionally written for proton targets. To obtain neutron structure functions, we exchange each quark PDF with that of the other quark in the same generation ($u(x) \rightarrow d(x)$, $d(x) \rightarrow u(x)$, $s(x) \rightarrow c(x)$, …) [8]. This exchange is possible because the u and d quarks have similar masses, and since protons are *uud* and neutrons are *udd*, the d quark in a proton reacts to strong interactions as the u quark in a neutron does, and vice versa. Quarks carry about half of the nucleon's momentum - gluons carry the rest [5]. Valence quarks carry most of the quark momentum and the light sea quarks carry more sea quark momentum than the heavy ones do. Once measured, linear combinations of structure functions can yield information such as the relative valence and sea quark momentum contributions [8].

3. Generalized Parton Distributions and Transversity

The European Muon Collaboration first measured that quark spin contributes a fraction (~13%) of the proton spin, implying that the rest of the spin is due to parton angular momentum and gluon spin [10]. The quark parton model only describes the longitudinal quark momentum distributions, so a more complete three-dimensional picture of parton behavior is needed to resolve this "spin crisis."

Form factors and PDFs can be extracted from more general mathematical objects called generalized parton distributions (GPDs). GPDs contain transverse quark position and momentum dependence in addition to the previously discussed form factors and PDFs. GPDs are derived from Wigner distributions, which are phase-space distributions for quantum mechanical systems applied to quarks and gluons. Wigner distributions contain the simultaneous position and momentum distributions to the maximum allowed precision and the relation between the two. Wigner distributions yield new quark distributions when integrated over different parameters. When integrated over position, Wigner distributions give rise to more general quark momentum fraction distributions called transverse momentum dependent parton distributions (TMDs), written as $q(x, k_t)$ and $q_T(x, k_t)$, where k_t is the transverse momentum, q is a quark longitudinal momentum PDF and q_T is a quark transverse momentum PDF. Wigner distributions integrated over k_t produce quantum phase-space distributions that can be used to find the 3D nucleon charge distribution at given x and the probability distribution of quarks with momentum x and impact parameter b. GPDs are used to describe these distributions [9].

There are eight GPDs for each quark flavor, written as $E, H, \widetilde{E}, \widetilde{H}, E_T, H_T, \widetilde{E}_T$, and $\widetilde{H}_T$. GPDs with no subscript have been studied experimentally through the processes that they affect. GPDs with the subscript T are called the "transversity" GPDs and are difficult to access

experimentally [2]. The word "transversity" refers to these GPDs and the effects they give rise to.

4. Coherent Charged Current Single Pion Production

Several transversity-dependent neutrino interactions were considered for simulation:

1. Coherent CC and NC single π production in carbon.

$\nu_\mu + {}^{12}C \to \mu^- + \pi^+ + {}^{12}C$
$\overline{\nu}_\mu + {}^{12}C \to \mu^+ + \pi^- + {}^{12}C$
$\nu_\mu + {}^{12}C \to \nu_\mu + \pi^0 + {}^{12}C$
$\overline{\nu}_\mu + {}^{12}C \to \overline{\nu}_\mu + \pi^0 + {}^{12}C$

The differential cross sections of these reactions depend on final state pion angle. The first reaction listed is the focus of our analysis. Coherent events preserve the target nucleus.

2. Coherent single η, η', ρ, and a_1 production in carbon.

$\nu_\mu + {}^{12}C \to \nu_\mu + \eta + {}^{12}C$ $\quad$ $\overline{\nu}_\mu + {}^{12}C \to \overline{\nu}_\mu + \eta + {}^{12}C$
$\nu_\mu + {}^{12}C \to \nu_\mu + \eta' + {}^{12}C$ $\quad$ $\overline{\nu}_\mu + {}^{12}C \to \overline{\nu}_\mu + \eta' + {}^{12}C$
$\nu_\mu + {}^{12}C \to \mu^- + \rho^+ + {}^{12}C$ $\quad$ $\overline{\nu}_\mu + {}^{12}C \to \mu^+ + \rho^- + {}^{12}C$
$\nu_\mu + {}^{12}C \to \nu_\mu + \rho^0 + {}^{12}C$ $\quad$ $\overline{\nu}_\mu + {}^{12}C \to \overline{\nu}_\mu + \rho^0 + {}^{12}C$
$\nu_\mu + {}^{12}C \to \nu_\mu + a_1 + {}^{12}C$ $\quad$ $\overline{\nu}_\mu + {}^{12}C \to \overline{\nu}_\mu + a_1 + {}^{12}C$

3. Strange reactions in hydrogen.

$\nu_\mu + p \to \mu^- + K^+ + \Sigma^+$
$\overline{\nu}_\mu + p \to \mu^+ + K^0 + \Sigma^0$ $\quad$ $\overline{\nu}_\mu + p \to \mu^+ + K^0 + \Lambda^0$
$\overline{\nu}_\mu + p \to \mu^+ + K^- + p$ $\quad$ $\overline{\nu}_\mu + p \to \mu^+ + \overline{K}^0 + n$

We chose to study $\nu_\mu + {}^{12}C \to \mu^- + \pi^+ + {}^{12}C$ events. This event type will be common in the MINERvA data and the neutrino event simulator we used can generate them without modification, unlike some of the other event types. A Feynman diagram is shown in Figure 2. The interesting kinematic variables are x, Q^2, $t = |t|$ (which are Lorentz-invariant), and φ, the pion azimuthal angle respect to the neutrino-muon plane in the lab frame (Figure 3). A

coordinate system is defined in this figure: c_1 is parallel to $\boldsymbol{q}$, c_2 is normal to the lepton plane, and c_2 is perpendicular to c_1 and c_3. The components of $\boldsymbol{p_\pi}$ along c_2 and c_3 are $p_2 = \boldsymbol{p_\pi} \cdot \hat{n}$ and $p_3 = \boldsymbol{p_\pi} \cdot (\hat{n} \times \hat{q})$, where $\hat{n}$ is normal to the lepton plane and $\hat{q}$ is the unit vector of $\boldsymbol{q}$. By geometry, $\varphi = \text{atan2}(p_3, p_2)$.

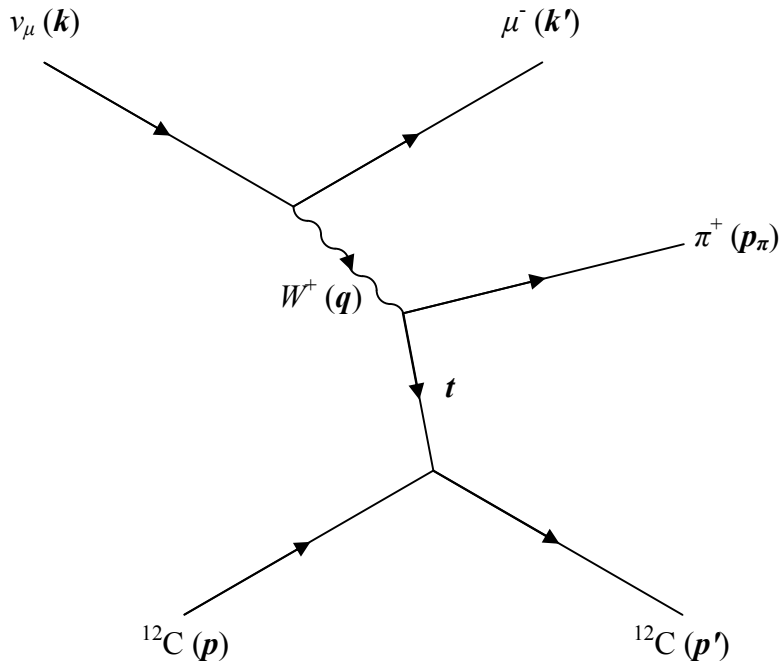

Figure 2: Feynman diagram of the $\nu_\mu + {}^{12}C \rightarrow \mu^- + \pi^+ + {}^{12}C$ reaction. Four-momenta are indicated in bold.

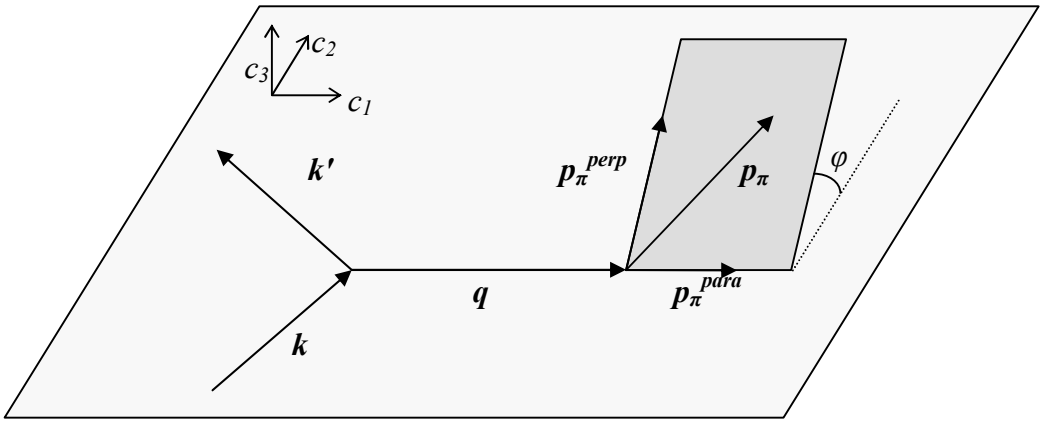

Figure 3: The geometric definition of φ in terms of momentum components. $\boldsymbol{k}$ and $\boldsymbol{k'}$ lie in the lepton plane (light grey), and the pion azimuthal angle φ is the angle that $\boldsymbol{p_\pi}$ is rotated up from the lepton plane about $\boldsymbol{q}$.

In [3], Ahmad, Goldstein, and Liuti include the differential cross section for exclusive π^0 electron scattering, which can be used for our reaction, as follows:

$$\frac{d^4\sigma}{d\Omega dE' d\phi dt} = \Gamma\left[\frac{d\sigma_T}{dt} + \varepsilon_L \frac{d\sigma_L}{dt} + \varepsilon\cos 2\phi \frac{d\sigma_{TT}}{dt} + \sqrt{2\varepsilon_L(\varepsilon+1)}\cos\phi \frac{d\sigma_{LT}}{dt} + h\sqrt{2\varepsilon_L(1-\varepsilon)}\sin\phi \frac{d\sigma_{L'T}}{dt}\right]$$

where h is the neutrino helicity (h = 1 for right-handed antineutrinos and h = –1 for left-handed neutrinos), $\varepsilon^{-1} = 1 + 2\left(1 + \frac{\nu^2}{Q^2}\right)\left(\frac{4\nu^2}{Q^2}\frac{1-y}{y^2} - 1\right)^{-1}$, $\varepsilon_L = \frac{Q^2}{\nu^2}\varepsilon$, $d\Omega$ is the incident neutrino solid angle, and the $d\sigma/dt$ terms are differential cross sections. The authors then numerically calculate the differential cross section contributions from two models: the GPD model and the Regge model. The GPD model describes the reaction as an interaction between partons, while the Regge model describes strong interaction scattering amplitudes [8]. Our goals are to simulate whether MINERνA will be sensitive to the terms sinusoidal in φ and if MINERνA will be able to distinguish between the two models, implying which model is reflected in the data.

Neutrino experiments boost our confidence in the quark parton model. Inelastic electron and neutrino scattering are consistently described by the quark parton model despite being dominated by different interactions (electromagnetic and weak, respectively). Neutrino-nucleon structure function measurements demonstrate the existence of sea quarks [8]. Neutrino events with charmed final state particles project out the $s(x)$ contribution to the nucleon momentum. Neutrino experiments can make similar contributions to transversity investigations. Transversity experiments search for differences in longitudinally polarized, transversely polarized, and unpolarized beam and target cross sections as the transversity signature [2]. Neutrino reactions are always polarized since neutrinos are left-handed are antineutrinos are right-handed.

Hardware, Software, and Methods

1. The MINERνA Experiment

MINERνA uses the NuMI (Neutrinos at the Main Injector) neutrino beam. NuMI produces the beam by directing the 120 GeV proton beam from the Fermilab Main Injector accelerator into a graphite target, producing showers of pions and kaons that decay to muon neutrinos. The pions and kaons are focused by two magnets and travel through a 700 m tunnel, where they decay to produce the neutrino beam [11]. The NuMI magnets can be moved to generate different neutrino energy fluxes, a low energy (LE) beam (3 GeV peak) and a medium energy (ME) beam (7 GeV peak) [1]. The neutrino beam is pulsed in 8 μs intervals, and the detector readout is synchronized with the beam to reduce the background signal [11].

The MINERνA detector lies about 100 m past the end of the decay tunnel directly in the path of the neutrino beam and is itself a neutrino target. Additional graphite, iron, and lead targets embedded in the detector and a liquid helium target in front of the detector will provide more target nucleus variety [1]. The NuMI beam is used in the MINOS (Main Injector Neutrino Oscillation Search) experiment, and the MINERνA detector is placed 2 m "upstream" of the MINOS near detector. The MINOS near detector can detect forward-going muons that MINERνA does not stop, enhancing its resolution. In the four years of planned operation, the MINERνA collaboration expects to collect 1.5×10^6 CC events, of which 8.9×10^4 are coherent CC single pion production events, and 4.4×10^4 coherent NC single pion production events [12]. Construction is scheduled to finish in early 2010, though the current installation is already collecting data.

The MINERνA detector consists of hexagonal cross section planes that lie perpendicular to the neutrino beam direction (Figure 4, 5). Most of the detector is a core of plastic scintillator

strips surrounded by other detectors. The strips have a triangular cross section (1.7 cm height, 3.3 cm width) and lie in the detector planes. Charged particles that pass through these strips emit photons, which are internally reflected in the strip until they are trapped in a wavelength-shifting fiber. The fiber then carries the photons to photomultipliers and photodetectors. The triangular strip cross section ensures that forward-going particles pass through two strips per plane, which results in better final state particle track reconstruction. The individual planes of strips are oriented at 60° from one to the next, allowing 3D track reconstruction [1].

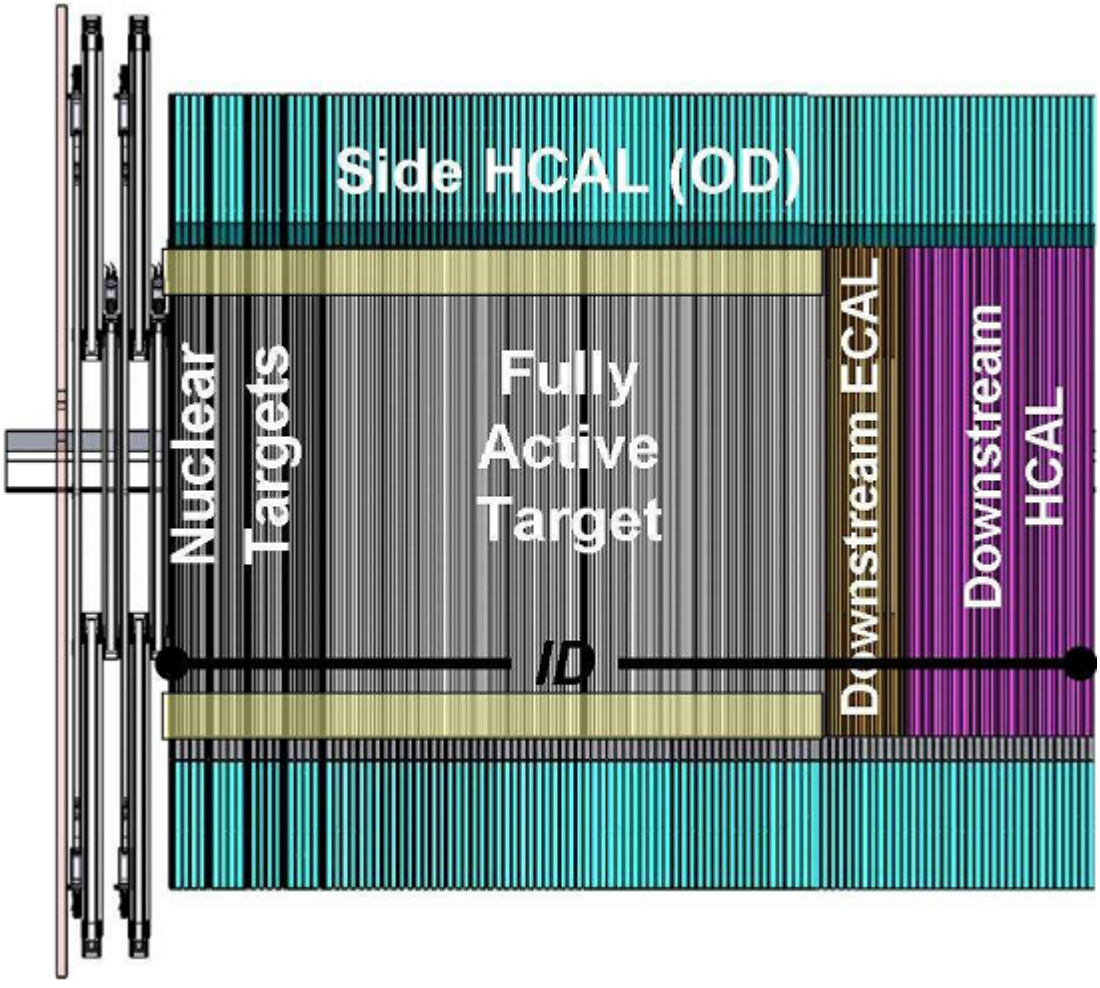

Figure 4: MINERvA detector side view. The plastic scintillator strips lie in the vertical planes labeled "Fully Active Target," and the neutrino beam enters from the left [1].

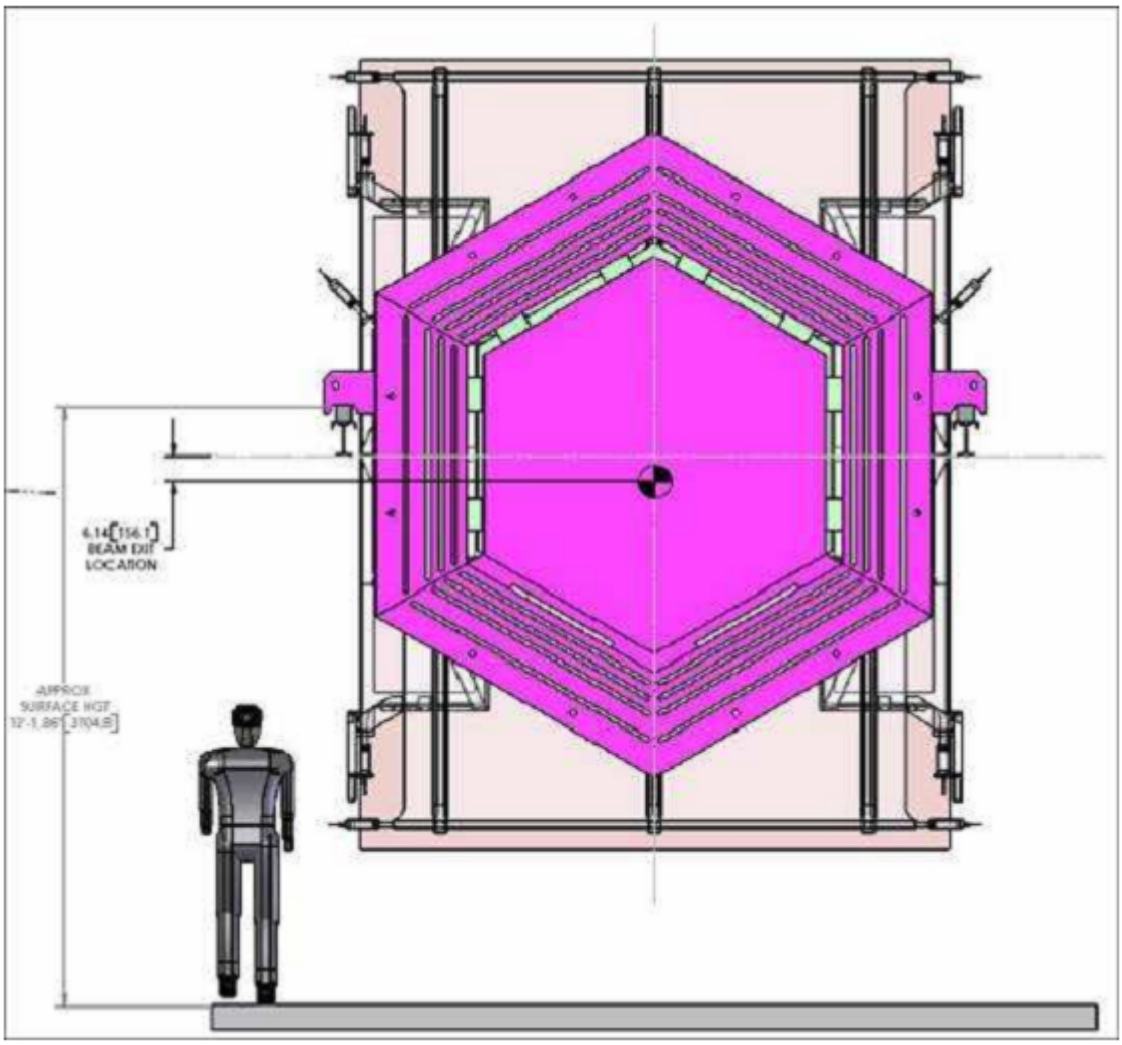

Figure 5: MINERvA detector rear view. [1]

The primary goal of MINERvA is to measure low energy neutrino cross sections for coherent single pion production, quasi-elastic scattering, strange and charm particle production, and resonant production [1, 12]. Such measurements will improve the measurements of other low energy neutrino beam experiments searching for neutrino oscillations and other fundamental physics. Nuclear effects, such as how final state particles are perturbed within the target nucleus, will be studied with the range of Z available (H, He, C, Fe, and Pb). The poorly known high x

PDFs and GPDs will also be studied [1]. Coherent single pion production is sensitive to transversity, so MINERvA could provide the first transversity data for neutrino reactions.

2. Simulation Methods

We simulated neutrino events using a software package called GENIE (Generates Events for Neutrino Interaction Experiments) [13]. GENIE is object-oriented and uses theoretical and empirical models, other simulation packages, and an analysis package written for particle physics applications called ROOT [14]. Given a set of parameters (target nucleus, incident neutrino energy distribution, event type, …), GENIE generates a list of neutrino events and associated kinematic parameters. GENIE neutrino event information is contained in an "event record" object with the initial, intermediate, and final state "particle" objects and objects containing interaction kinematics and process information. We used GENIE to generate neutrino event files and modified a test program written by Costas Andreopoulos (the primary GENIE author) to loop over the events, extract and modify the events, and perform the analysis with ROOT. We set GENIE to simulate neutrino events with either monoenergetic neutrinos or neutrinos with energies distributed according to MINERvA neutrino beam configurations. GENIE also produced either all event types or only coherent CC single pion production events to avoid generating unnecessary events. The simulations and analyses were run remotely on the Tufts University MINOS computer (http://minos.phy.tufts.edu/), which runs Scientific Linux.

GENIE event record objects contain the event x, Q^2, and t, and we implemented a method for calculating φ. GENIE uses a cross section model by Rein and Sehgal [15] to simulate exclusive coherent CC single pion events, but since this model does not include φ dependence, GENIE chooses a random φ between 0 and 2π. When testing the φ calculation logic, GENIE was

modified to produce pions of constant φ, but the analysis code was calculating variable φ. This led us to find a mistake in GENIE, which we corrected in our installation. To align the pion, we define a primed frame, where the $x'z'$ plane is the lepton plane and z' is along $\boldsymbol{q}$. Setting the pion momentum in the primed frame is convenient: the unrotated pion momentum is $\boldsymbol{p_\pi}$ = ($\boldsymbol{p_\pi}^{perp}$, 0, $\boldsymbol{p_\pi}^{para}$) and the rotation by φ is a rotation about z'. To set φ and rotate back to the original frame (with the incident neutrino along z), GENIE now does the following:

1. Rotate $\boldsymbol{p_\pi}$ about the z-axis by the chosen φ.
2. Rotate about the y-axis by θ_q, the zenith angle of $\boldsymbol{q}$ in the unprimed frame.
3. Rotate about the z-axis by φ_q, the azimuthal angle of $\boldsymbol{q}$ in the unprimed frame.

These operations point the z' axis along $\boldsymbol{q}$ while keeping x' in the lepton plane. The geometry is drawn in Figure 6.

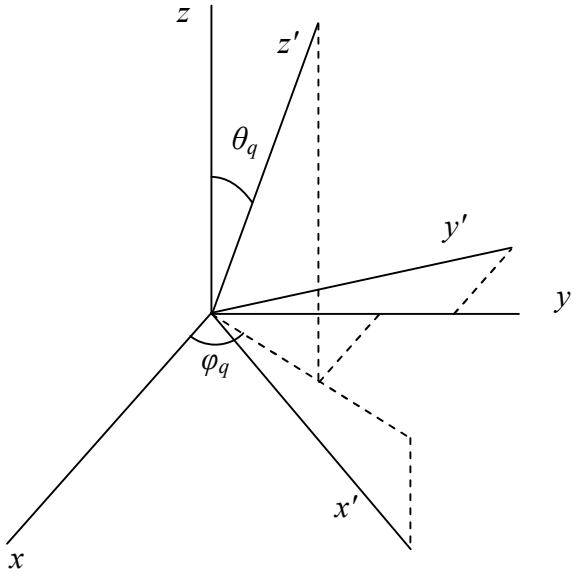

Figure 6: Primed and unprimed coordinate system geometry. The y' axis lies in the xy plane and is normal to the lepton ($x'z'$) plane. z' is along $\boldsymbol{q}$.

3. Event Reconstruction and Detector Smearing

Routines introducing detector particle angle resolution, particle energy resolution, and event reconstruction effects were added to the analysis code to simulate how raw data is perturbed in an experiment and what the effect is on x, Q^2, t, and φ. To reconstruct events from measured final state muon and pion four-momenta, we make two assumptions:

1. The incident neutrino direction is known. In GENIE, incident neutrinos travel in the z direction.
2. The final state ^{12}C nucleus energy is just the rest mass, i.e. the energy component of $\boldsymbol{t}$ is zero. This is a good approximation because the ^{12}C nucleus has a small recoil momentum (< 1 GeV/c), so there is not much energy transfer.

Applying conservation of four-momentum to the reaction $\nu + {}^{12}C \rightarrow \mu + \pi + {}^{12}C$ gives us

$$\begin{pmatrix} E_\nu \\ 0 \\ 0 \\ E_\nu \end{pmatrix} + \begin{pmatrix} m_C \\ 0 \\ 0 \\ 0 \end{pmatrix} = \begin{pmatrix} E_\mu \\ p_{x\mu} \\ p_{y\mu} \\ p_{z\mu} \end{pmatrix} + \begin{pmatrix} E_\pi \\ p_{x\pi} \\ p_{y\pi} \\ p_{z\pi} \end{pmatrix} + \begin{pmatrix} m_C \\ p_{Cx} \\ p_{Cy} \\ p_{Cz} \end{pmatrix}.$$

This results in four linear equations in neutrino energy E_ν, and final state ^{12}C three-momentum p_{Cx}, p_{Cy}, and p_{Cz}. Solving yields $E_\nu = E_\mu + E_\pi$, $p_{Cx} = -(p_{\mu x} + p_{\pi x})$, $p_{Cy} = -(p_{\mu y} + p_{\pi y})$, and $p_{Cz} = -(p_{\mu z} + p_{\pi z}) + E_\mu$.

Particle detectors have finite particle angular and four-momentum measurement resolution, introducing statistical errors when measuring these parameters. We call this detector event "smearing;" perfectly sharp angle and four-momenta are smeared into distributions due to detector measurement inaccuracies. The MINERvA detector has 0.5° angle resolution, 10%

muon four-momentum resolution, and 18% / $\sqrt{E}$ pion resolution (E is the pion energy in GeV), as calculated with a program called GEANT, which simulates the detector response to particles traveling through it [1, 16]. We assume the angle and energy distributions to be Gaussian and uncorrelated, allowing us to implement them in the analysis code separately. This also means that four-momentum smearing is done by multiplication by a constant factor; smearing momentum components individually changes the particle angle, and angle perturbations are taken care of by a separate angle smearing routine.

The analysis program smears the events before reconstructing them. Both processes modify GENIE particle object four-momenta but not the GENIE event record x, Q^2, and t, so these variables were read out before smearing and reconstruction and manually recalculated afterward. φ was calculated both times with the same routine. We can then compare the relative differences between the true and perturbed φ to determine that MINERvA is sensitive enough to the sinusoidal variations in differential cross section.

4. Pion φ Transversity Dependence

The cross sections calculated in [3] are being implemented in GENIE. Instead of GENIE calculating the differential cross sections during run time, they are precalculated and stored in tables of x, Q^2, and t. GENIE uses a posterior probability of φ: given that an event occurs with certain kinematic parameters, what is the probability distribution of φ? GENIE determines φ by sampling the phase space of φ and the probability of φ (differential cross section) until it finds a combination that works.

Only one of the cross section tables for the Regge model is currently implemented (x = 0.13, Q^2 = 1.3 GeV^2, -2 GeV^2 < $|t|^2$ < 0), so GENIE picks φ independently of x and Q^2. In the full

simulation, GENIE will perform an interpolation for both models and will eventually calculate the relevant differential cross sections during run time, though this may be impractical if it significantly slows down event generation.

Results

1. Smearing and Reconstruction Test Results

The GENIE-generated events were smeared and reconstructed in the analysis code to determine whether MINERνA could resolve features of the GPD and Regge models of pion φ-dependent differential cross section. An obvious quantity to study these perturbations is the fractional difference between true and perturbed kinematic variables: $(V_{true} - V_{pertrubed}) / V_{true} = \Delta V / V$, where V is x, Q^2, or t. For φ, the calculated quantity is $\Delta\varphi / \pi$ since the difference in φ is more fundamental than the original φ. The analysis code was run with detector smearing disabled to see if our assumption that $\boldsymbol{t}$ has no energy component is reasonable. The reconstructed $\Delta V / V$ were found to be essentially or exactly zero, which is to be expected for φ and t. $\boldsymbol{k}$ and $\boldsymbol{k'}$ define the lepton plane, and since the former has a known direction and the latter is measured, the lepton plane and rotation axis $\hat{q}$ are reconstructed exactly. $\boldsymbol{p_\pi}$ is also exact, so the reconstructed φ is identical because the geometry for calculating φ is identical. When calculating t, GENIE uses the same assumption as in the reconstruction (the final state ^{12}C has a rest mass energy, or $\boldsymbol{t}$ carries no energy component). The reconstructed t therefore equals the original GENIE t. We can still test the assumption by estimating the error in the final state ^{12}C energy. Given a typical $|t|$ of 0.2 GeV/c (3 GeV ν_μ-C coherent CC single pion production) and assuming that t is a three-momentum transfer, the final state ^{12}C four-momentum is (E, 0.2 GeV/c). By special relativity,

$$E = \sqrt{(mc^2)^2 + (pc)^2} = 11.180 \text{ GeV},$$

where m = 12 u = 11.178 GeV/c^2 is the ^{12}C rest mass and p = 0.2 GeV/c. E is less than 0.1% larger than m, so the assumption holds at typical t. Both x and Q^2 had essentially zero deviation from the true values. While the reconstruction routine was found to introduce no perturbations, it remains in the analysis program event loop because it applies momentum conservation to the ν_μ and ^{12}C four-momenta after smearing.

When simulating detector smearing, the ΔV / V distributions for x, Q^2, and t were asymmetrical, with x being particularly skewed (Figure 7). Examining the asymmetry due to each of the three smearing possibilities shows that this is primarily due to the pion four-momentum smearing (Figure 8). These figures were made with uniform φ distributions.

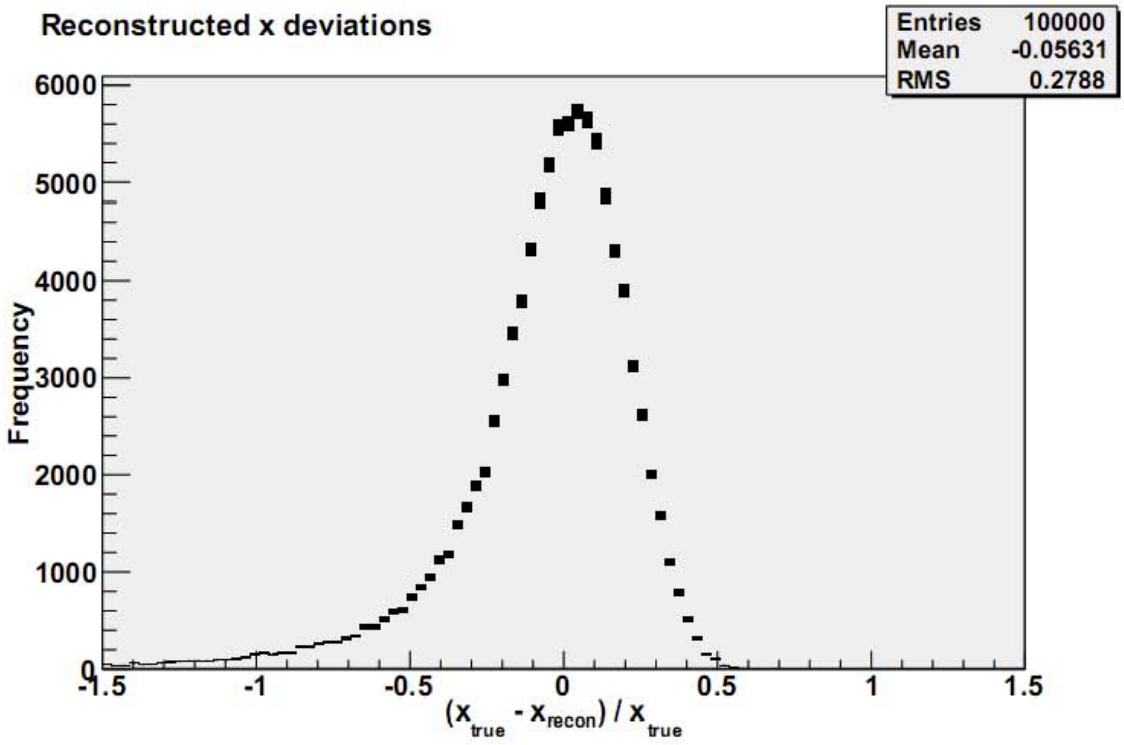
Reconstructed x deviations
Entries 100000
Mean -0.05631
RMS 0.2788
Frequency
6000
5000
4000
3000
2000
1000
0
-1.5
-1
-0.5
0
0.5
1
1.5
(x_true - x_recon) / x_true

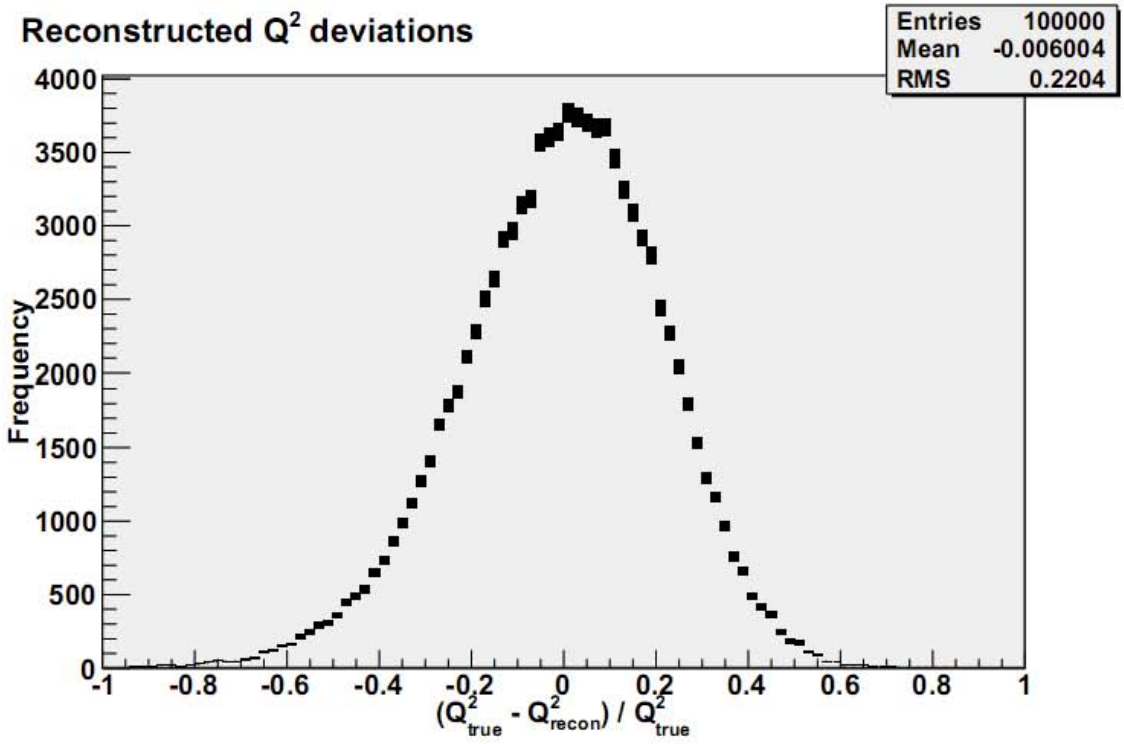
Reconstructed Q² deviations
Entries 100000
Mean -0.006004
RMS 0.2204
Frequency
4000
3500
3000
2500
2000
1500
1000
500
0
-1
-0.8
-0.6
-0.4
-0.2
0
0.2
0.4
0.6
0.8
1
(Q²_true - Q²_recon) / Q²_true

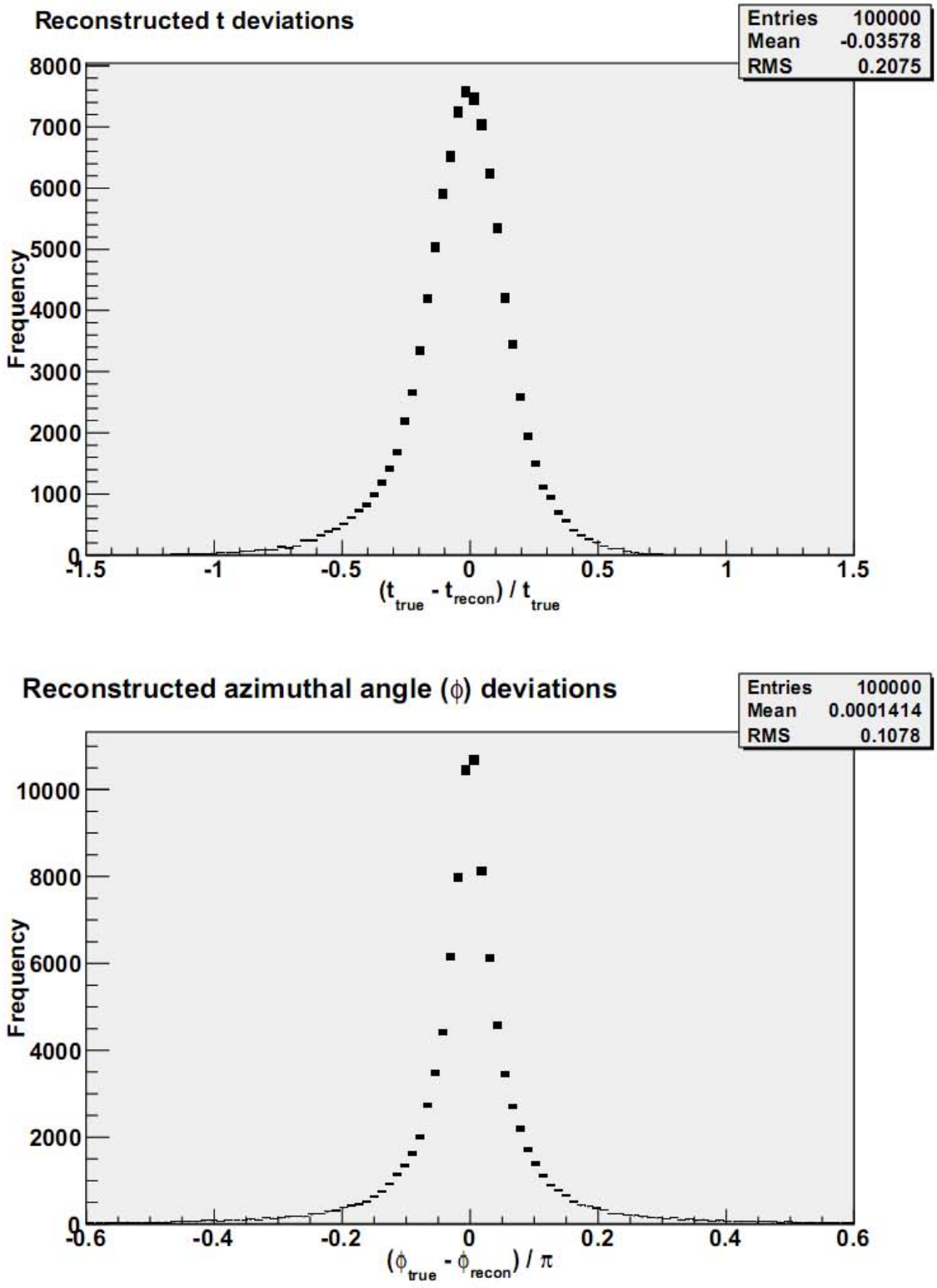

Figure 7: $\Delta V / V$ plots for 1 GeV ν_μ CC coherent single pion production (100,000 events). Notice the slight Q^2 and t asymmetry and the strong x asymmetry.

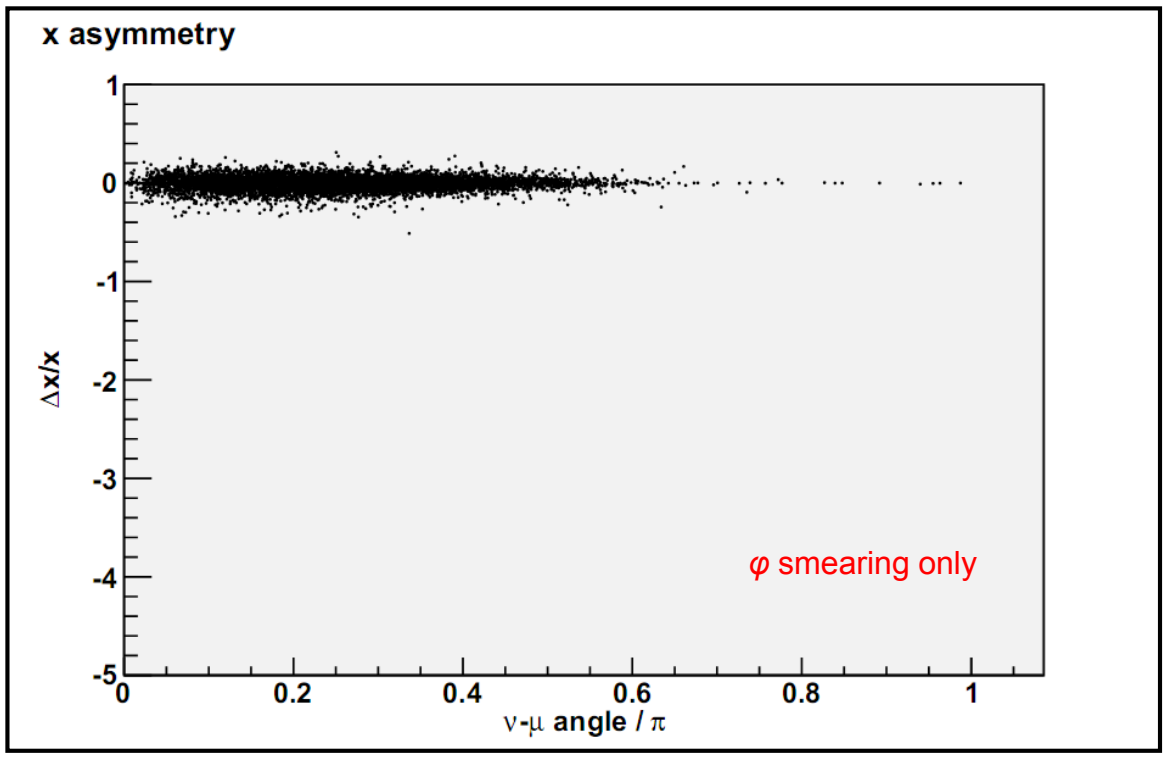
x asymmetry
Δx/x
ν-μ angle / π
φ smearing only

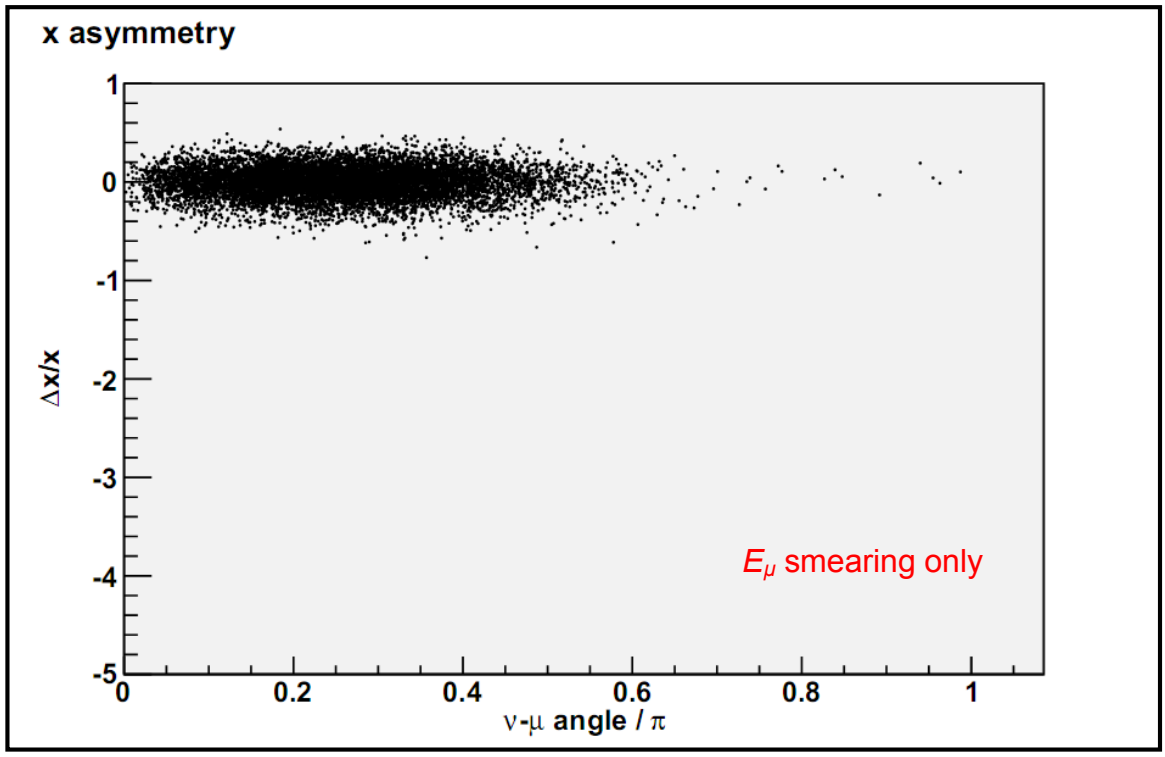
x asymmetry
Δx/x
ν-μ angle / π
E_μ smearing only

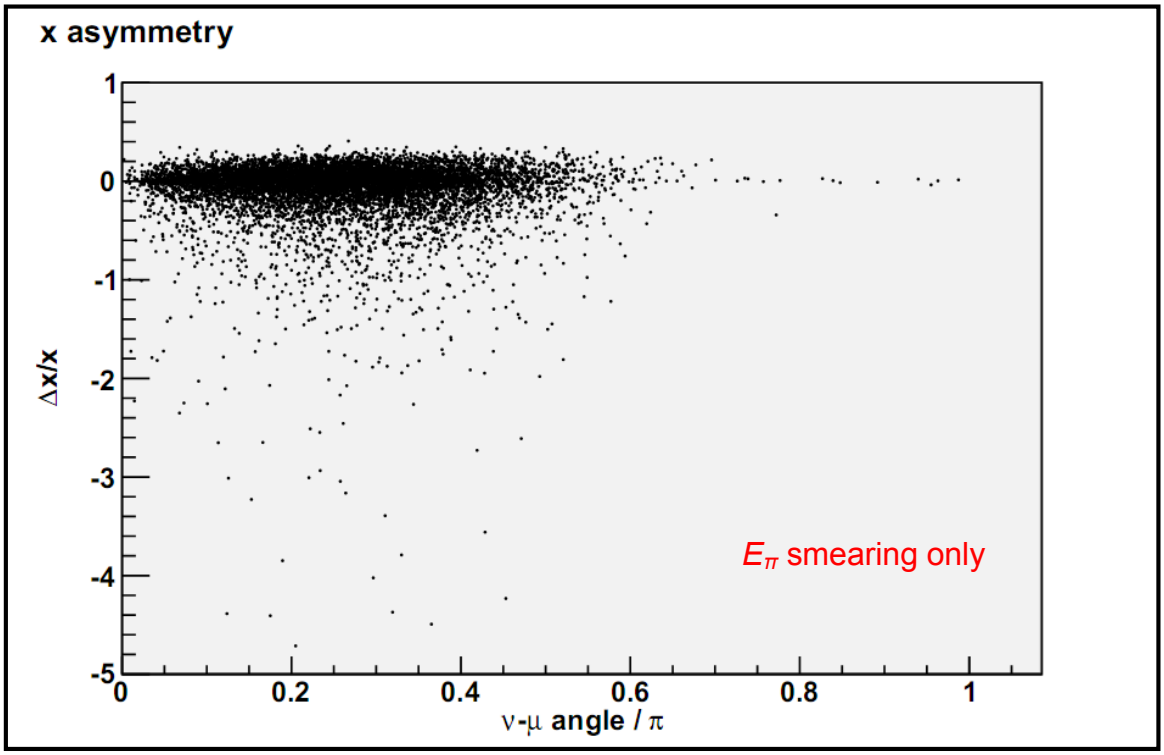

Figure 8: Δx / x as a function of final state muon angle for 1 GeV ν_μ CC coherent single pion production (10,000 events). The asymmetry in Figure 7 is caused by the pion four-momentum smearing.

The root mean square (RMS) of ΔV / V measures the widths of the distributions in Figure 7 and indicates how accurate these V are after smearing. The $\Delta\varphi$ / π RMS in Figure 7 and in tests with other energies indicates that MINERvA can resolve φ to 0.1π-0.3π radians. This suggests that MINERvA will be sensitive to the φ-dependent coherent CC single pion production differential cross section, which has sinusoidal features of order 0.5π. Direct tests with the cross section models implemented in GENIE are necessary because they will include the perturbations in the other kinematic variables and the contributions of the various sinusoidal terms.

To test whether detector precision strongly affects φ resolution, we examined how $\Delta\varphi$ / π varies with each detector resolution and with energy. The analysis program was modified to vary each smearing parameter individually over four values while keeping the others at their default

(MINERνA detector) values. We analyzed three event files (1, 3, and 10 GeV neutrinos) twelve times (four for each smearing parameter) and some results are plotted in Figure 9. As we might expect, less precise detectors measure φ with more error. The coherent CC single pion production cross section decreases in $Q^2 = 4E_\nu E_\mu \sin^2(\theta / 2)$, so muons (and hence pions) are more forward-going at higher energies and have closer trajectories. Small angular perturbations are more significant when the two momenta are closer together, which is reflected in Figure 9 as an increase in fractional uncertainty with energy.

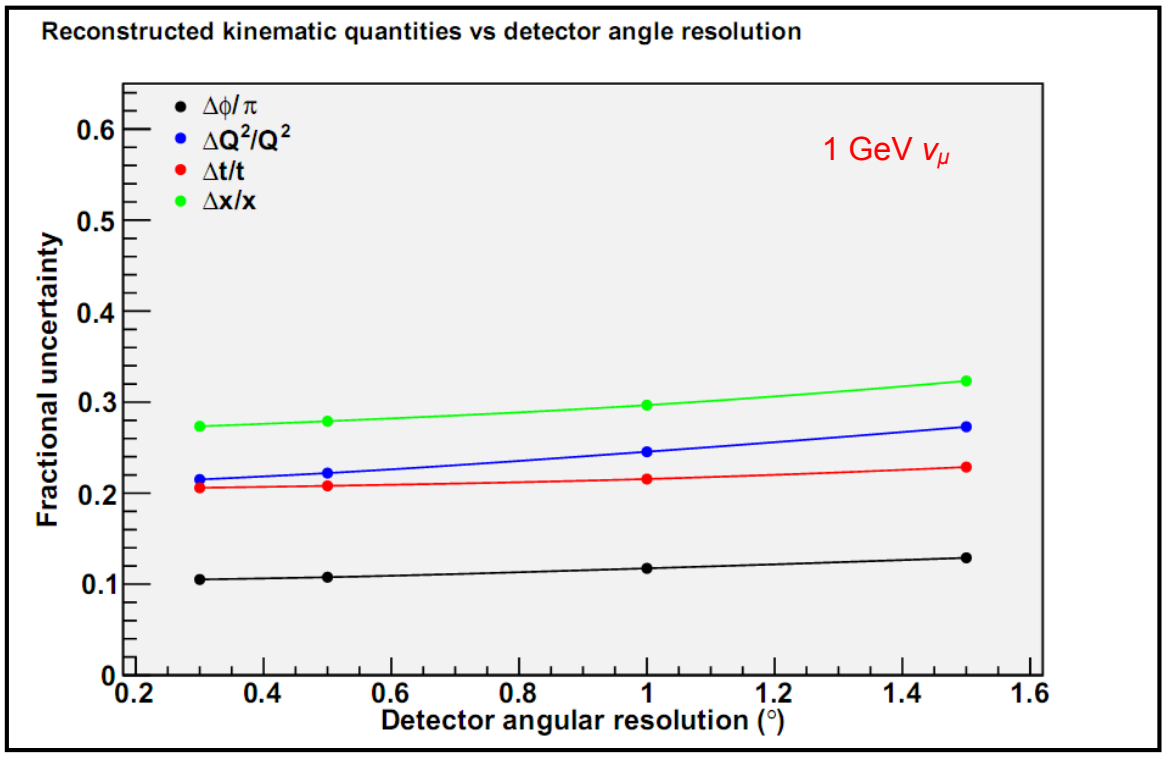
Reconstructed kinematic quantities vs detector angle resolution
Δϕ/π
ΔQ²/Q²
Δt/t
Δx/x
1 GeV ν_μ
Fractional uncertainty
Detector angular resolution (°)
0
0.1
0.2
0.3
0.4
0.5
0.6
0.2
0.4
0.6
0.8
1
1.2
1.4
1.6

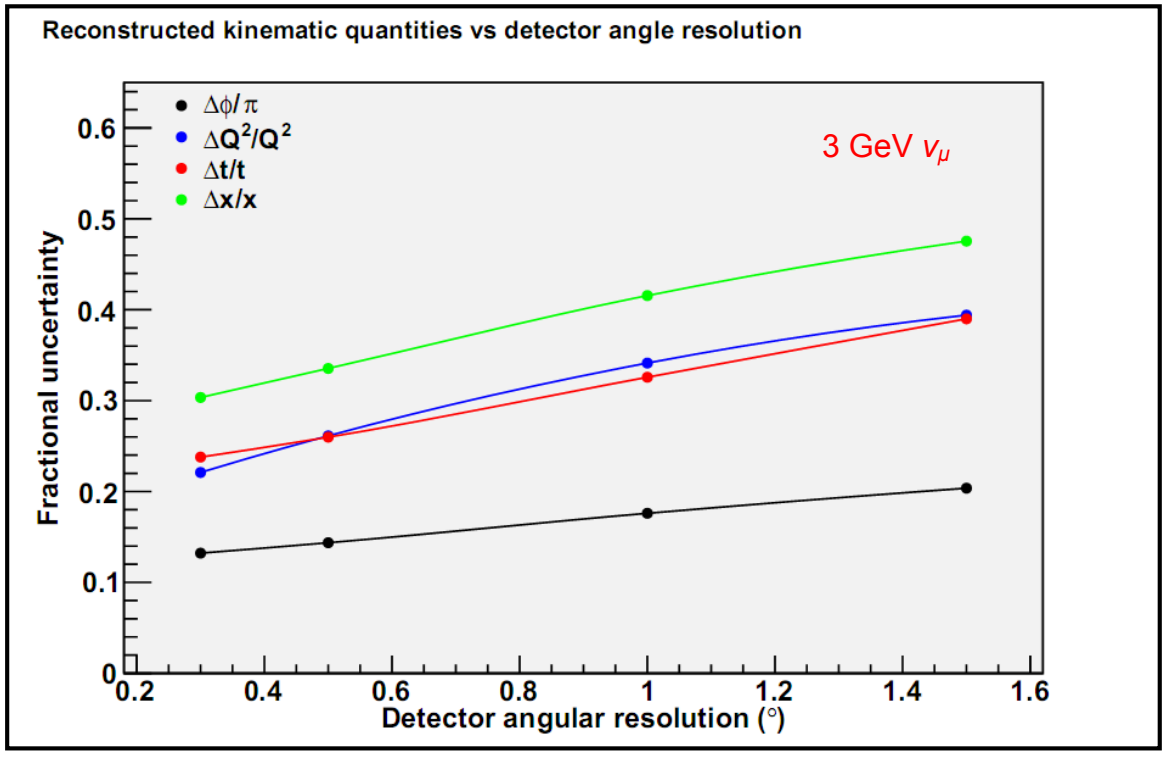
Reconstructed kinematic quantities vs detector angle resolution
Δϕ/π
ΔQ²/Q²
Δt/t
Δx/x
3 GeV ν_μ
Fractional uncertainty
Detector angular resolution (°)
0
0.1
0.2
0.3
0.4
0.5
0.6
0.2
0.4
0.6
0.8
1
1.2
1.4
1.6

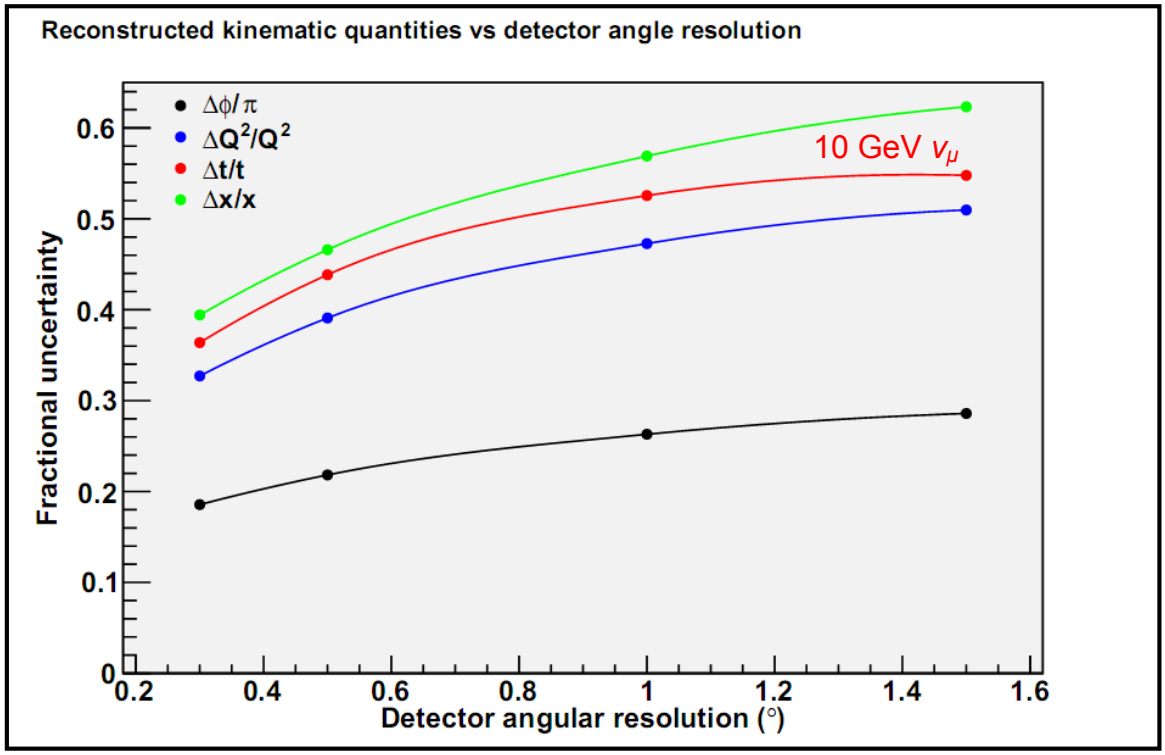

Figure 9: Kinematic variable fractional uncertainty (ΔV / V RMS) at three ν_μ energies (100,000 events). Error bars due to statistics are too small to include.

2. Testing Transversity-Dependent φ

The simplified Regge model implementation was tested in a 100,000 event "combined" MINERvA flux, with the LE to ME fluxes merged in a 1:3 ratio as in the four year run plan. A histogram showing event frequency in φ is included in Figure 10 and shows a clear cos(2φ) pattern in event rate. The histogram was fitted with the function $a + b\cos(2\varphi) + c\cos(\varphi) + d\sin(\varphi)$ with the ratio of coefficients $a : b : c : d = 53.7 : 18.5 : -2.47 : 1$ (0.32%, 1.3%, 10%, and 21% relative error, respectively). We can check these values by estimating the constant and sinusoidal coefficients in the differential cross section. Using average kinematic parameters (x = 0.081, Q^2 = 0.21 GeV^2, ν = 1.6 GeV^2, y = 0.24, t^2 = -0.028) and the cross sections in the table for the characteristic t, the ratio of coefficients is $a : b : c : d = 36.3 : 19.5 : -3.61 : 1$, which is quite similar.

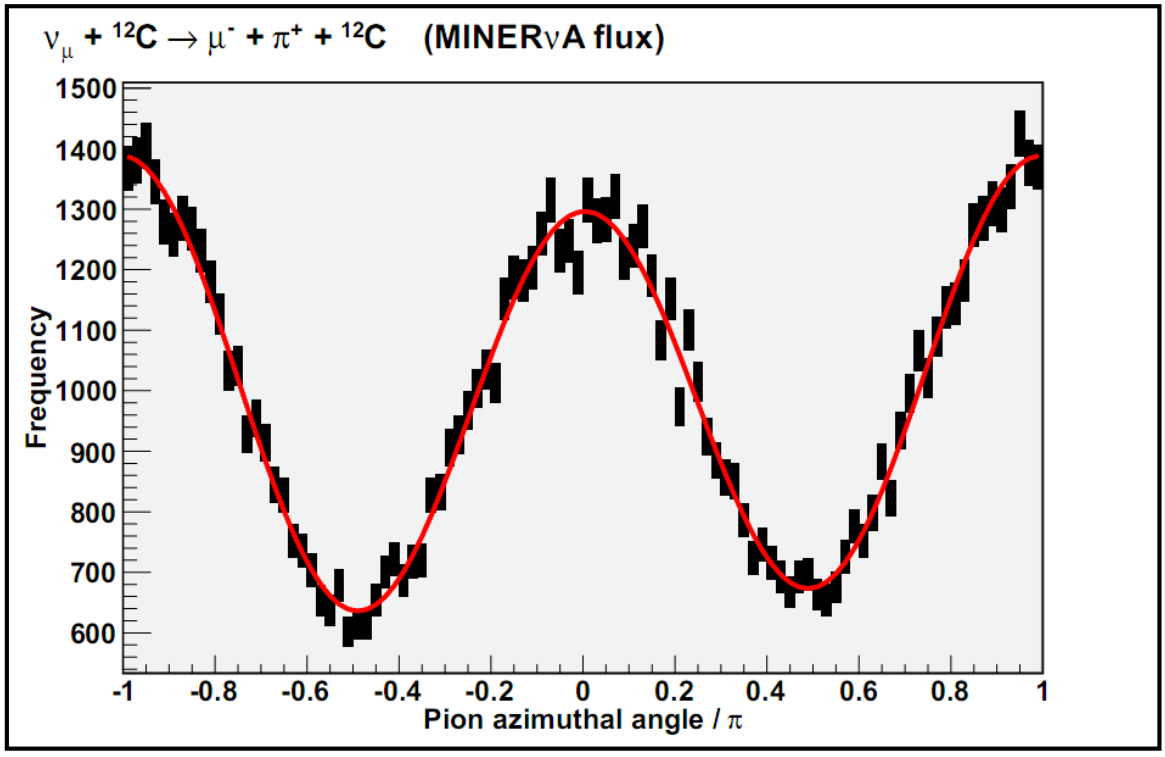

Figure 10: Histogram of reconstructed Regge model φ for 100,000 events with the combined MINERνA flux. The red curve is a fitted function of the form $a + b\cos(2\varphi) + c\cos(\varphi) + d\sin(\varphi)$ and shows $\cos(2\varphi)$ dominance among the sinusoidal terms.

Though we have not simulated a similar result in the GPD model, we claim that the GPD model event rate will be independent of φ. Figure 11 includes a plot of calculated cross section contributions to the differential cross section for the two models at $x = 0.13$, $Q^2 = 1.3$ GeV^2 done by authors of [3]. The Regge model $\cos(2\varphi)$ term is a significant contribution to the total cross section (approximately the sum of the dotted curves when ignoring other kinematic variable dependence) at $t^2 \approx -0.03$ GeV^2. The constant term dominates the total GPD cross section, implying largely flat φ dependence. MINERνA can therefore distinguish between the two models because the Regge model predicts a strong $\cos(2\varphi)$ contribution to the event rate and the GPD model predicts almost no φ dependence. This qualitative difference is partially confirmed by the

Regge model test in Figure 10, though a similar simulation with the GPD model will fully confirm it.

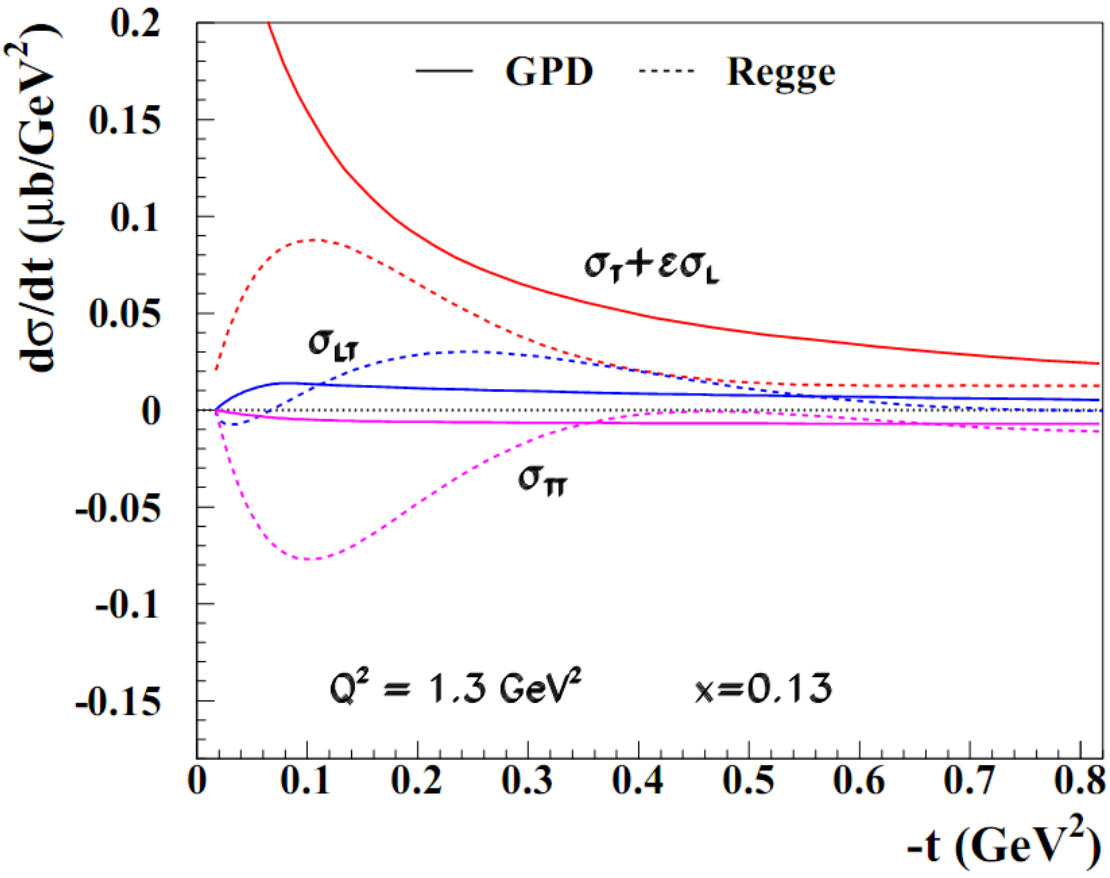

Figure 11: Cross section contributions for the GPD (solid curves) and Regge (dotted curves) models. Red indicates the constant term *a*, pink the cos(2φ) term *b*, and blue the cos(φ) term *c*. The sign of the Regge model σ_{TT} is opposite from that of the cross section table used in GENIE, which is a sign error in either the figure or the table [3].

Conclusions and Future Work

We simulated coherent CC single pion production events ($\nu_\mu + {}^{12}C \rightarrow \mu^- + \pi^+ + {}^{12}C$) in MINERvA to study whether MINERvA will be sensitive to the transversity-dependent differential cross section. With a partial Regge model implementation in place and qualitative GPD model cross section arguments, we find that MINERvA will be able to differentiate

between the two models, as the Regge model predicts a strong cos(2φ)-dependent event rate and the GPD model predicts an event rate uniform in φ. We also find that the MINERνA detector resolution yields φ measurements with 0.1π-0.3π radian error.

This work can be expanded on several fronts to refine these findings. The obvious next step is to complete the Regge model implementation and include the GPD model implementation in GENIE. This will involve either using more cross section tables for precise interpolation or calculating cross sections exactly while GENIE is generating events. The cross sections used are also taken from an electromagnetic electron scattering theory, so the theory must be modified to neutrino scattering. We can simulate how to extract the cross section contributions from the data. We fitted the Regge model φ-dependent event rate (Figure 10) with constant *a*, *b*, *c*, and *d*, though since these coefficients depend on kinematic variables, a more elaborate scheme is required for cross section measurement. A full detector simulation should replace the simulated smearing portion of the simulation to more accurately portray the detector effects. Contamination from other event types in the coherent CC single pion production sample (events that falsely appear to be of this type) must also be included, as this will be addressed in the MINERνA analysis. Finally, only one transversity-dependent reaction was pursued from a list of potential reactions. Studying other event types can shed light on additional neutrino transversity measurements.

Bibliography

1. "The MINERvA Technical Design Report", MINERvA collaboration internal document 700-v28 (2008).

2. H. Avakian *et al.*, "Deeply Virtual Compton Scattering at 6 GeV with transversely polarized target using the CLAS detector", New Research Proposal to Jefferson Lab PAC 33.

3. S. Ahmad, G.R. Goldstein, S. Liuti, "Nucleon Tensor Charge from Exclusive π^0 Electroproduction", arXiv:0805.3568v2 (2009).

4. Fermi National Accelerator Laboratory, "Inquiring Minds: The science of matter, space, and time", available at http://www.fnal.gov/pub/inquiring/matter/madeof/index.html.

5. D. Griffiths, "Introduction to Elementary Particles", John Wiley & Sons (1987).

6. W.-M. Yao *et al.*, "Review of Particle Physics", Journal of Physics G: Nuclear and Particle Physics **33** (2006).

7. A. Das, T. Ferbel, "Introduction to Nuclear and Particle Physics", World Scientific (2003).

8. R. Devenish, A. Cooper-Sarkar, "Deep Inelastic Scattering", Oxford University Press (2004).

9. X. Ji, "Generalized Parton Distributions", Annual Review of Nuclear and Particle Science, Vol. 54, Annual Reviews (2004).

10. European Muon Collaboration, "An investigation of the spin structure of the proton in deep inelastic scattering of polarised muons on polarised protons", Nuclear Physics **B328** (1989).

11. "NuMI Technical Design Handbook", available from http://www-numi.fnal.gov/numwork/tdh/tdh_index.html.

12. B.P. Ziemer, "MINERvA: νN Scattering", MINERvA collaboration internal document 3575-v1, (April 2009).

13. C. Andreopoulos *et al.*, "GENIE Neutrino Monte Carlo Generator", available at http://genie-mc.org/.

14. "ROOT: A Data Analysis Framework", available at http://root.cern.ch/drupal/.

15. D. Rein, L.M. Sehgal, "Coherent π^0 Production in Neutrino Reactions", Nuclear Physics **B223** (1983).

16. "GEANT - Detector Description and Simulation Tool", available from http://wwwasd.web.cern.ch/wwwasd/geant/.